Calculation of SANS intensity for polyethylene: effect of varying fold planes and fold plane roughening

Charles M. Guttman, Edmund A. DiMarzio, and John D. Hoffman
National Measurement Laboratory, National Bureau of Standards, Washington, DC 20234, USA
(*Received* 17 *September* 1980)

The intensity of the small angle neutron scattering (SANS) for polyethylene crystallized in the lamellar habit from the melt at large supercoolings is calculated for $\mu=0.01$ to $\mu=0.14$ [$\mu=(4\pi/\lambda)\sin(\theta/2)$]. Computations are made on models which allow various amounts and types of chain folding and varying degrees of 'tight' or 'regular' folds. The models that fit the SANS data best have folding along lattice planes in which the stem separation is larger than 0.5 nm (5 Å) or which allow for fold plane roughening on a variety of fold planes. the 'leapfrog' type folds mentioned by Sadler were also considered, and a possible cause for their existence suggested. As an example, the variable cluster model gives a good account of the SANS data with the surface roughening suggested by nucleation theory with fold planes [110], [200], and [310], or a mixture. Even though the conditions of crystallization used in preparing the SANS specimens (large supercoolings) were conducive to the maximum surface disorder, the probability of 'tight' or 'regular' folding, p_{tf}, was found to be ~ 0.7 for the best models. This corresponds closely to the theoretical lower bound $p_{tf}=2/3$ which is rigorous for the case of non-tiled stems. The probability of strictly adjacent re-entry in a single specified fold plane, p_{ar}, was ~ 0.4 to ~ 0.7 depending on the particular model chosen. The best models fit not only the SANS data, but also the liquid and crystal density, degree of crystallinity, and characteristic ratio (or radius of gyration). None of the models show the density anomaly inherent in the switchboard or random re-entry models of Yoon and Flory.

INTRODUCTION

Small angle neutron scattering (SANS) has been used to characterize the average configuration of a single chain in a lamellar semicrystalline system[1-7]; with this technique one may study the question of the character of the crystal–amorphous interfaces. A low concentration of deuterated chains are mixed with a protonated matrix (or *vice versa*) then crystallized and the intensity of single chain scattering estimated. SANS has been done on semicrystalline samples of polyethylene (PE)[1-4], polypropylene[5], polystyrene[6] and polyethylene oxide[7]. In this paper we shall only consider data on melt grown polyethylene systems. All of the PEH–PED specimens studied by neutron scattering were crystallized from the melt by rapid cooling to prevent isotopic segregation. Crystallization under such conditions of large supercooling is conducive to the maximum disorder in the fold surface, so specimens formed in this way may be thought of as presenting a worse case for chain folding.

In earlier papers in this series Guttman *et al.*[8] and Hoffman *et al.*[9] proposed models for chains in semicrystalline melt crystallized polyethylene which fit the SANS data, obtained on such material, fairly well. These models, called the variable cluster and central core models, were similar to those proposed earlier by Hoffman *et al.*[10] and were shown to be consistent with kinetic data. These models had a large fraction of adjacent folding but also some nonadjacent folding. In calculating scattering curves for these models it was assumed that chain folding occurred on the [110]* or [200] fold plane.

The variable cluster model and the central core model with folding on the [110] or [200] fold plane were criticized by Yoon and Flory[11] as having too high a SANS intensity for $\mu=0.08$ to $\mu=0.14$.

In this paper, we show that one can fit the SANS intensity data more closely by considering chain conformations which allow for stem separations in the crystal larger than 0.5 nm (5 Å).

Previous papers have tried to characterize the amorphous–crystalline interface. One quantity which has been used to characterize this interface is the probability of adjacent re-entry, p_{ar} [8,9]. This was defined as the fraction of stems which return adjacent to the previous crystal stem in the same chain with only a few segments used in the interfacial region (8–20 for PE). In this work we define two other quantities which also shall characterize the surface. As we shall discuss later, one often has stems which return near adjacent or next near adjacent but always with tight folds (loops using only a few segments — see *Figure 1*). The fraction of stems which return near adjacent or next near adjacent is p_{aar}, the probability of close adjacency. Finally the quantity which measures the sum of adjacent, near adjacent or next near adjacent stems all with tight folds, shall be called the probability of tight folding, p_{tf}. We have:

$$p_{tf}=p_{ar}+p_{aar} \tag{1}$$

Each grouping of adjacent, near adjacent and next near adjacent stems connected by tight folds shall be called a cluster. The average cluster size for an infinite molecular weight chain, $\langle n_c\rangle$ is related to p_{tf} by

* In this paper [110] always refers to the 110 fold plane.

0032-3861/81/050597-12$02.00

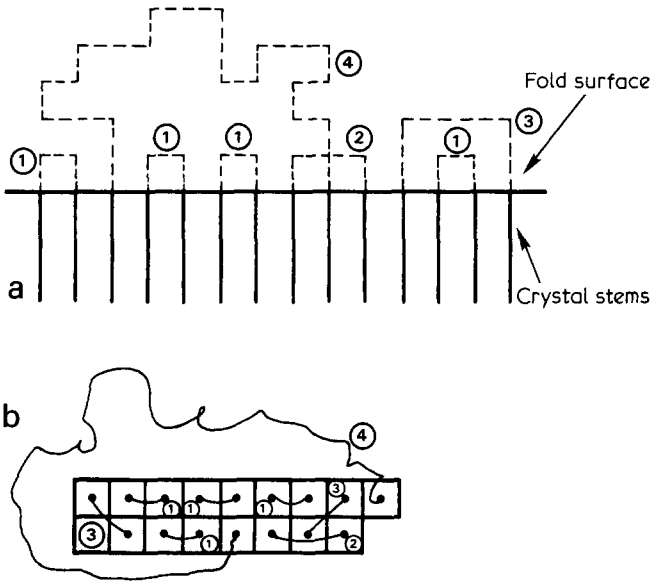

Figure 1 Schematic representation of different types of folding (a) a variety of tight loops (regular folds) and a loose loop is shown in a single given fold plane. Folds marked 1 are adjacent folds and are counted in p_{ar}. Folds marked 2 and 3 are near adjacent folds and are counted in P_{aar}. Folds 1, 2 and 3 all contribute to p_{tf}. Loose loops like 4 are not counted in p_{tf}. (b) A variety of regular folds and loose loops shown on the plane perpendicular to the fold plane. Folds marked 1 are adjacent folds and are counted in p_{ar}. The fold marked 2 is an example of a next near adjacent fold. Folds marked 3 are examples of tight folds resulting in fold plane roughening. Folds 1, 2 and 3 count in p_{tf}. The loose loop marked 4 is not counted in p_{tf}

$$\langle n_c \rangle = (1 - p_{tf})^{-1}$$

Models with p_{tf} at zero or near zero are usually called 'switchboard' or 'random re-entry' models[11-13]. In these models the chains in the amorphous region all obey random walk statistics. Each crystal stem of a chain exits from the crystal at some point and re-enters at a point which is determined by random walk statistics. The point of re-entry is generally thought to occur some distance from that of its emergence.

In the more general 'adjacent re-entry model' as each crystal stem exits the crystal phase it chooses whether it will return to the crystal in a few steps (fold) or whether it will exit into the amorphous phase. The fraction of stems which return directly to the crystal adjacent to the previous stem in the chain is measured directly by p_{ar}.

The general adjacent re-entry model can yield very different surfaces for the crystal–amorphous interface depending on the fraction of stems of a chain which return adjacent. If p_{ar} or p_{tf} is near unity, that is, each stem is next to the next stem in the chain, then the fold surface is expected to be relatively smooth[14] and we have the 'fully adjacent model'. This limit, that of complete adjacency, is the antithesis of the 'random switchboard model'.

In the other extreme, when the p_{tf} is near zero, we have the 'switchboard model'. It is found to be impossible to set up a model in which p_{tf} is zero. Guttman *et al.*[8], have shown that one switchboard model of Yoon and Flory[12] has about 20% accidental adjacency.

The general adjacent re-entry model with different fractions of adjacency can span the extremes from the 'fully adjacent stem model' to the nearest possible approximation to the 'switchboard model'. A determination of the p_{tf} should help one decide on the kind of interface that exists between crystal and amorphous phase.

In earlier theoretical work on SANS, Yoon and Flory[12] calculated the SANS intensity of single chains in semicrystalline polyethylene (PE) matrices for 'switchboard' or 'random re-entry' models. These models, although they fit the intensity of the neutron scattering data from very small angles out to $\mu = 0.14$ [$\mu = (4\pi/\lambda)\sin(\theta/2)$ where θ is the scattering angle and λ is the neutron wavelength] and fit the characteristic ratio, were criticized[8] as being incorrect because they either (1) yielded density profiles which showed too high a density in the amorphous regime (and thus, the incorrect crystallinity); or (2) had a density profile in which the crystalline–amorphous interface density was twice as large as the crystalline density. *Figure 2* shows the density profile of two of the Yoon and Flory models along with the density profile of a model of the semicrystalline polymer with a fraction of adjacency of ~ 0.7. The unreal density profile of models like the Yoon and Flory model were predicted earlier in a qualitative manner for the switchboard model by Frank[15]. A number of recent papers[16,17] have analytical estimates of the density errors in such models.

Guttman *et al.*[8] have proposed single chain models of melt crystallized PE with fractions of adjacency greater than 0.5. These models simultaneously fit the SANS intensity, the characteristic ratio, the crystallinity and the density profile. As mentioned earlier these models have been criticized by Flory[11] as having too high a SANS intensity at higher μ. Hoffman *et al.*[9], however, have shown that a best overall simultaneous fit to all data (that is, the overall averaged fit of the SANS intensity, density, crystallinity and characteristic ratio), is obtained with those models which have over 50% adjacency.

Despite the arguments of Hoffman *et al.*, the previous models by Guttman *et al.* could be improved in that they predict scattering intensities at intermediate μ higher than the observed SANS intensity on polyethylene. The possibility that the experimentally observed intensity may itself be in error will not be discussed in detail in this paper. We will presume that the SANS data on melt crystallized PE are acceptable and we will suggest models which have an acceptable density profile, correct crystallinity, correct characteristic ratio and which fit the entire SANS curve to $\mu = 0.14$. These models — 'variable cluster' and 'central core' types, both of which are in the general classification of the general adjacent re-entry model — all fit the scattering and other data with a substantial fraction of adjacent re-entry.

This paper will present models which fit the data even better than our previous models[8]. To do this, we shall compute the SANS intensity for models of PE chains in a semicrystalline matrix which include the effects of (1) fold planes which are different than those assumed previously, (2) surface roughening due to the high undercooling required for the sample preparation, and (3) a 'skipping' or 'leapfrog model'[18] of the fold surface which has been shown to avoid the density anomaly of the switchboard model[19].

We shall discuss briefly the available SANS data on melt crystallized PE; briefly review the Monte Carlo calculations and models; show the effects of different fold planes on the SANS intensity; model fold surface roughness and calculate its effects on SANS intensity. The scattering from the 'leapfrog' or 'wicket' model variations will also be presented.

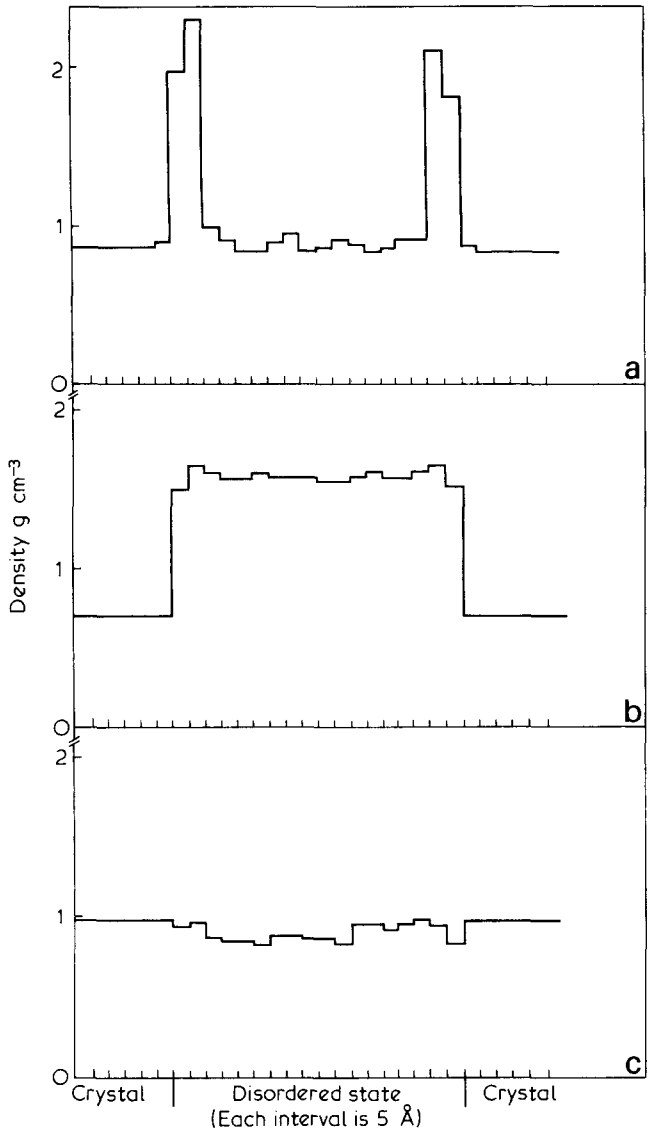

Figure 2 (a) Density of Yoon Flory irregular reentry model $p_{es} = 0.3$ $p_{en} = 0.7$. Density is calculated assuming the average density of a semicrystalline polymer sample is 0.95 g cc^{-1}. The fact that the density is not symmetric around the centre of the disordered phase gives an idea of the error in the computation of density. High peaks in the interfacial regime are a result of the reflecting wall condition imposed by Yoon and Flory. The low value of the crystalline density is caused by the low fractional mass crystallinity, χ_m, obtained from the Monte Carlo calculation as opposed to the higher fractional volume crystallinity, χ_v, imposed upon the model by the assumed lamellar spacings. (b) Density of Yoon and Flory adjacent reentry $\gamma = 1$ model using same assumptions as in *Figure 2a*. The low crystal density is due to χ_m being less than χ_v. (c) Density of central cluster model with 7 stems in a row ($N = 2500$). Assumptions are same as *Figure 2a*

TREATMENT OF INTENSITY OF SANS DATA

SANS data in the range $\mu = 0.01$–0.14 on semicrystalline melt crystallized polyethylene have been reported by Schelten *et al.*[1], Sadler and Keller[2], Bai[4] and Stamm *et al.*[3]. In an earlier paper we estimated the single chain scattering function $P_N(\mu)$ for the data of Schelten *et al.* sample A6Q by

$$P_N(\mu) = \left(\frac{\partial\Sigma}{\partial\Omega}\right)_\mu \Big/ \left(\frac{\partial\Sigma}{\partial\Omega}\right)_{\mu=0} \qquad (2)$$

where $(\partial\Sigma/\partial\Omega)_\mu$ is the differential scattering cross section obtained from their *Figure 7* and $(\partial\Sigma/\partial\Omega)_{\mu=0}$ is their zero angle intensity obtainable from their *Figure 4*.

A Kratky type function, similar to that used by Yoon and Flory[12] will be used to display both the experimental and calculated results. We compute:

$$F_N(\mu) = N\mu^2 P_N(\mu) \qquad (3)$$

where N is the molecular weight divided by 16 for PED. This choice of function is convenient for a Monte Carlo calculation where N is a starting parameter in the program. A comparison of the Monte Carlo calculation with the experimental data requires that we know the molecular weight of the sample material. In the Schelten *et al.* work, two weight average molecular weights are given for their sample A6Q. One obtained by g.p.c. (60 000) and one by SANS (46 000). Which molecular weight is proper to use in the data analysis is not clear, but others[1,8,12] generally have analysed the data using the g.p.c. molecular weight values.

In this paper we shall display $F_N(\mu)$ computed from the Schelten data using each of the molecular weights. The intensity scaled with the g.p.c. molecular weight is referred to as the 'g.p.c. scaled Schelten data' while the intensity scaled with the SANS molecular weight is called the 'SANS scaled Schelten data'.

Recently Sadler[2] and Stamm *et al.*[3], have criticized the use by Yoon and Flory and Guttman *et al.* of the g.p.c. scaled Schelten data suggesting that the correct data to use is the SANS scaled Schelten intensity. In *Figure 3* the SANS intensities computed by these two methods are displayed as well as the data of Sadler and Keller, Stamm *et al.*, and of Bai[4]. The data of Bai and of Stamm *et al.* agree with the SANS scaled Schelten data and with Sadler and Keller's data on 97 000 molecular weight melt crystallized materials. Sadler and Keller's data on other melt-crystallized samples are generally considerably lower.

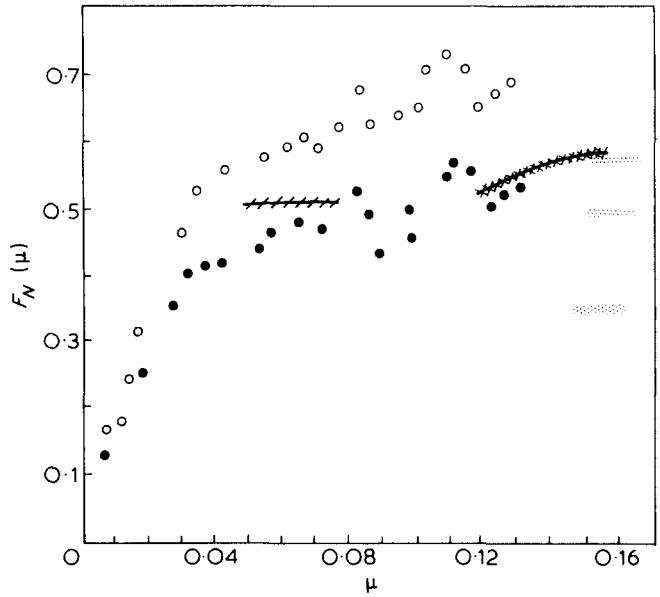

Figure 3 Single chain Kratky function, $F_N(\mu)$ *versus* μ, displaying the various experimental results on PEH–PED melt crystallized. Open circles (○) are the g.p.c. scaled Schelten *et al.* SANS intensity data. Dots (●) are the SANS scaled Schelten *et al.* SANS intensity data (⁎) is Bai's data. The crosshatched solid line (⁎⁎⁎) is Stamm *et al.* data. The speckle are Sadler *et al.* data

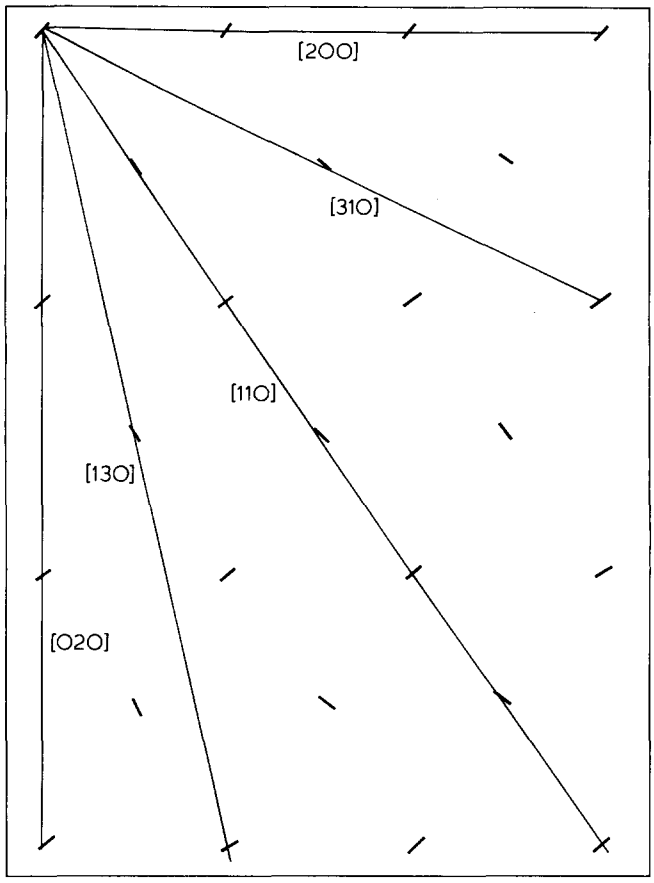

Figure 4 Projection of PE lattice perpendicular to stem axis. Chains shown as (/). Lines are possible fold planes

In the paper we shall use the phrase 'the scattering intensity of some model fits the SANS scaled Schelten data' as shorthand for the statement that the intensity from the model fits the SANS scaled Schelten data as well as the Bai, the Stamm and the Sadler and Keller data for 97 000 molecular weight.

Bai has shown that the regime $\mu = 0.04$ and above is independent of concentration or other chain effects. It is our opinion, however, that the scatter in the data from various workers along with the uncertainties in the data discussed previously do not yet permit us to choose any one set of data above the others. Thus, we shall display all the gathered data without bias and show how various models can fit the data.

MONTE CARLO MODELS AND CALCULATIONS

Local chain characterization

In this section, we shall describe the local characterization of the chain in our Monte Carlo model. In following sections, we shall describe the overall chain morphology as the chain passes from crystalline to amorphous phases. In the calculations we shall follow the same local description of the chain which Yoon and Flory have used. Therefore the description which follows will characterize our chains as well as theirs.

In the paper of Yoon and Flory[12] the C–C bond and the C–C–C skeletal bond angles were given the value $l = 0.154$ nm (1.54 Å) and $\theta = 68°$, respectively. A lamellar structure was set up for the computation within the computer; the crystal phase was taken as 16 n, (160 Å) thick and the amorphous phase 9 nm (90 Å) thick. This corresponds to the sample of Schelten *et al.*[1] who used a 65% crystalline sample with a long spacing of 25 nm (250 Å). Within each crystal lamella the chains were all given *trans* conformations. In the amorphous phase the chain took on the conformations given by the rotational isomeric state model of polyethylene as discussed by Flory[20]. As in the Yoon and Flory paper we used the Flory statistical weight matrix with Flory's values of $\sigma = 0.54$ and $\delta = 0.088$. Each chain starts with a stem.

The nature of the transit through the amorphous–crystal interface should be noted in the model. The chain leaves the crystal phase in a *trans* configuration. It may, however, enter the crystal phase from any previous, *trans*-, *gauche*+ or *gauche*− configurations. Also, its angle of entrance into the crystal face is not controlled. The chain may enter at a skimming angle.

In contrast to our previous work[8] and the calculations of Yoon and Flory[12], we have established a polyethylene lattice for our crystal phase. In our present calculations the polymer chains were forced to come into the lattice on a lattice site. *Figure 4* shows the projection of that lattice perpendicular to the stem axis. We have also rejected any chain which had crystal stems occupying the same lattice sites — that is, we have invoked excluded volume for the crystal stems. Stamm *et al.*[3], have shown that crystal stem exclusion affects the intensity of the SANS at intermediate angles for a Yoon and Flory type model. The effect of this change on our previous results is negligible.

NEW CHAIN MORPHOLOGICAL MODELS

Folds and high fractions of adjacent re-entry

In a previous paper[8] we described a variety of chain morphological models which, in the main, have slightly higher $F_N(\mu)$ values ($\sim 20\%$) at $\mu = 0.14$ than the g.p.c. scaled Schelten data. All models had been developed to avoid the density defect of the Yoon and Flory models discussed previously. All our models showed the proper crystallinity and the correct radius of gyration or C_n. All models showed a considerable amount of adjacent re-entry (60–80% of the crystal stems are adjacent). The fact that these earlier calculations were only slightly above the SANS intensity data suggests that an improved model, which fits the SANS data better, will still retain substantial adjacent re-entry.

Two separate models were presented in our earlier paper[8]. The central core model is a model of a chain in a semicrystalline matrix in which the central portion of the chain was highly folded and the ends were partially folded. This model is shown schematically in *Figure 5*. A model with no folding in the ends was used by Guenet *et al.*[6], (their ACA model) to explain the SANS intensity on semicrystalline polystyrene. No detailed Monte Carlo calculations on the ACA model were presented by Guenet *et al.* Further support for the central core model has been offered by Hoffman *et al.*[9] who suggested that this model is consistent with the kinetic nucleation models that involve reptation[21] in the melt. A number of authors[9,22,23] have shown that reptation in the liquid state of polyethylene was rapid enough, under the influence of the force of crystallization, to allow the accretion of a number of adjacent stems on the growth substrate.

The other model discussed in our earlier paper[8] was called the variable cluster size model. In this model, as

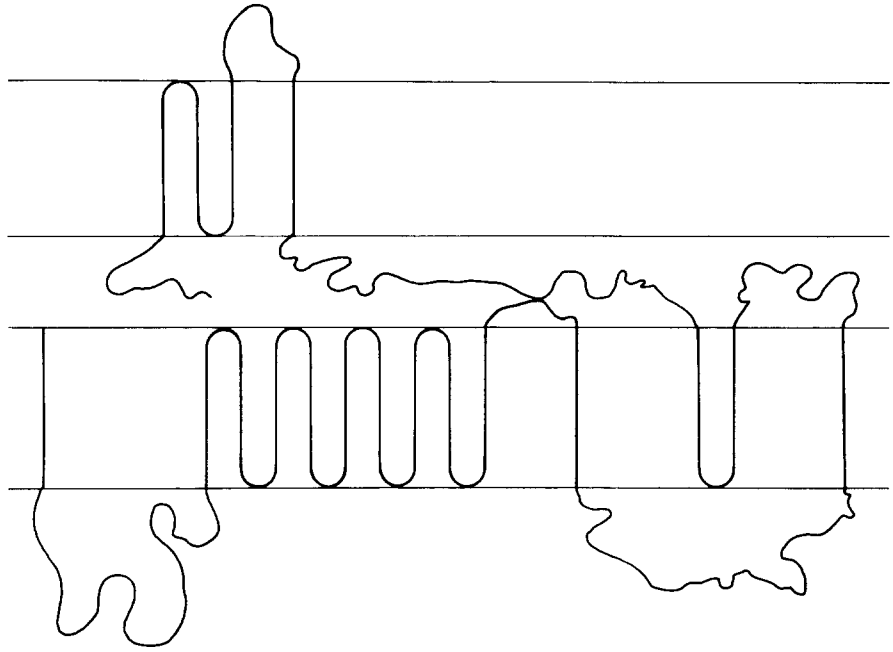

Figure 5 Schematic representation of central core model with 9 stems in the central core

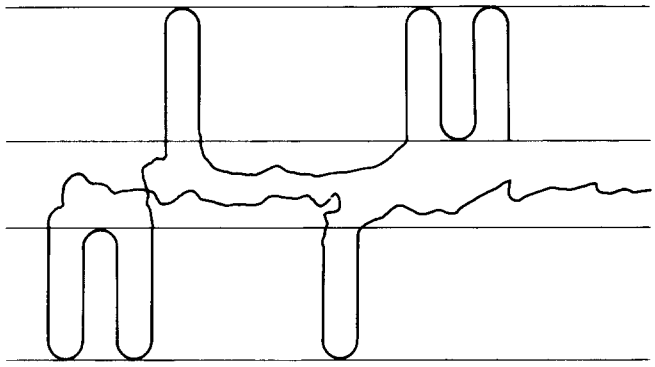

Figure 6 Schematic representation of variable cluster model

each stem finishes its traverse of the crystal phase, it has a probability p_{stem} of making a fold and probability $1-p_{\text{stem}}$ of going into the amorphous phase. Such a model allows for folding but the size of each folded stem cluster is variable. A model similar to this — the 'Garland model' — was used by Guenet *et al.* to explain other data on semicrystalline polystyrene. A schematic representative chain from this model is shown in *Figure 6*. The rate of reptation in the polyethylene is quite sufficient to form the clusters of stems of the size characteristic of the variable cluster model.

As in the previous paper we shall compute the Kratky scattering function $F_N(\mu)$ as well as the characteristic ratio of the radius of gyration, C_n, the density and the crystallinity for these models. In our earlier paper[8] we discussed how the Yoon and Flory procedure of laying down the chain leads to loops as small as five PE segments. Since a tight fold is seven segments or more we have, in the spirit of the discussion in our previous paper, replaced all loops of 10 segments or less with adjacent folds. Our calculations shall differ from before in that we shall have stem exclusion, a correct lattice for the crystal phase, and we shall allow (1) different fold planes (2) surface roughness (3) a leapfrog or wicket-like model of tight adjacent and near adjacent loops. These three modifications shall be discussed later.

Table 1 Properties of models and experiment

	Experimental	Variable cluster	Central core
Crystallinity	65% (Schelten)	64–68%	64–68%
Characteristic ratio $C_N = \frac{6\langle S^2\rangle}{(1.54)^2 N}$	8.7	9–12	9–11
Probability of tight folding, p_{tf}		0.6–0.8	0.6–0.8
Probability of adjacent re-entry, p_{ar}		0.6–0.8 (models with varying fold plane)	0.6–0.8 (models with varying fold plane)
		0.34–0.4 (models with roughening or leapfrogging)	0.35–0.4 (models with roughening or leapfrogging)

We present the calculated characteristic ratio and crystallinity for each of these models in *Table 1* along with their experimental values from Schelten *et al.*[1]. There is little variation in the characteristic ratio, the crystallinity and the density profile of these models as we make the three variations discussed above. Also listed in *Table 1* are the probabilities of tight near folding, p_{tf} and p_{ar} for the models. For most models p_{tf} is near 0.73 and in all cases they are greater than 0.6. The ranges of values given in *Table 1* reflect not only variations between different models but also the 'experimental' Monte Carlo error. This error has been discussed in some detail earlier[8] for all properties considered here. The discussion and the magnitude of the error estimates made in that paper hold also for this work.

The density profile for all the models presented in this paper is similar to the profile presented in *Figure 2c*.

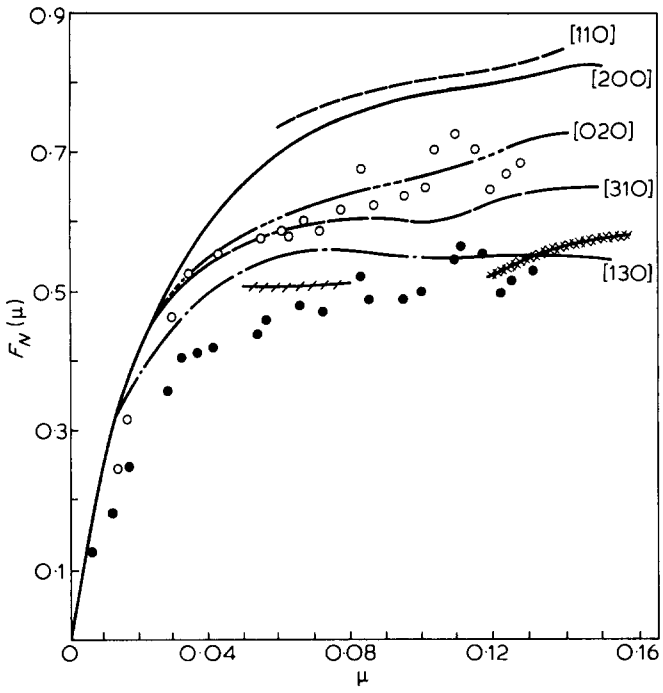

Figure 7 Scattering displayed as $F_N(\mu)$ *versus* μ for variable cluster model for the [110], [200], [020], [310] and [130] fold planes

EFFECT OF CHANGING SPACINGS BETWEEN ADJACENT STEMS

In our previous paper[8] and in the work of Yoon and Flory[12] on PE, a 0.5 nm (5 Å) spacing between adjacent stems on a square lattice in the plane perpendicular to the stem axis was used. This spacing assumes folding on the [200] or perhaps the [110] fold plane (see *Figure 4*). The [110] and [200] fold planes are the fold planes generally accepted as the growth fold planes for single crystals of PE from morphological arguments (see Khoury and Passaglia[14], and Keller[24]).

These conclusions on fold planes are generally arrived at by studying the lozenge shaped single crystals grown from dilute solutions at small undercoolings. However, as one lowers the crystallization temperature the shape of the single crystal grown from solution changes. The texture of the lamellar growing edge roughens and the growing edge does not necessarily exhibit a single distinct growth plane. Bassett and Keller[25] described the appearance of [310] growth surfaces along with the [110] fold surface in highly undercooled single dendritic crystals. This suggests that at high undercooling the polymer may, even in the melt, favour this growth plane. Thus, it seems from evidence on single crystals from solution that the fold plane changes as one changes the temperature of crystallization. In fact, one seems to go from fold planes with stems close to [110] at high temperature (and slow growth rates) to fold planes with more separated stems, e.g. [310], at lower temperatures (and higher growth rates).

We note in this connection that Guenet *et al.*[6] have shown from their SANS analysis that isotactic-(i)-polystyrene crystallizes from dilute solution with considerable adjacent re-entry along the [330] fold plane.

Little is known of the growth plane in melt crystallized samples. One usually assumes that the [110] or the [200] growth plane predominate. The infra-red work of Krimm[26] suggests [200] folding from data on samples of quenched PED in PEH. However, he cannot rule out [020] folding from his evidence alone[26]. The latter folding places the stems much further apart 0.74 nm (7.36 Å) than the [110] or [200] folding.

The above discussion leads us to no definitive choice of fold plane for the quenched melt-crystallized samples of polyethylene that we are modelling. Thus, we offer here the scattering intensity for models using a variety of fold planes. We chose the [110], [200], [310], and [020] fold planes because they have been suggested by others for either solution-grown and melt-grown material. For symmetry and completeness we present scattering models from the [130] fold plane also. *Figure 4* shows these fold planes.

The scattering data for the variable cluster size model with these various fold planes chosen is shown in *Figure 7*. All models shown here have probabilities of adjacent re-entry, p_{ar} of 0.6 to 0.7 and have characteristic ratio, C_n, and crystallinity close to the experimental values. It is seen from *Figure 7* that the [310] and [020] folding planes fit the g.p.c. scaled Schelten data best while the [130] plane does well on the SANS scaled Schelten, the Stamm *et al.*, the Bai data and the higher Sadler data.

Figures 8 and *9* show scattering intensity calculations for the central core model where folding has again been allowed along these various fold planes. As before we see that the data is best fitted by the models which used fold planes with spacing of stems wider than 0.5 nm (5 Å).

The fact that the data are best fitted with models using fold planes with stem separations of greater than 0.5 nm (5 Å) suggests that the rapid quenching which is necessary to avoid segregation of the deuterated sample may be the cause of the adjacent folding along planes which require longer spacing between stems. We observe, however, that the introduction of fold planes other than [110] or [200] in polyethylene does not imply that the substrate com-

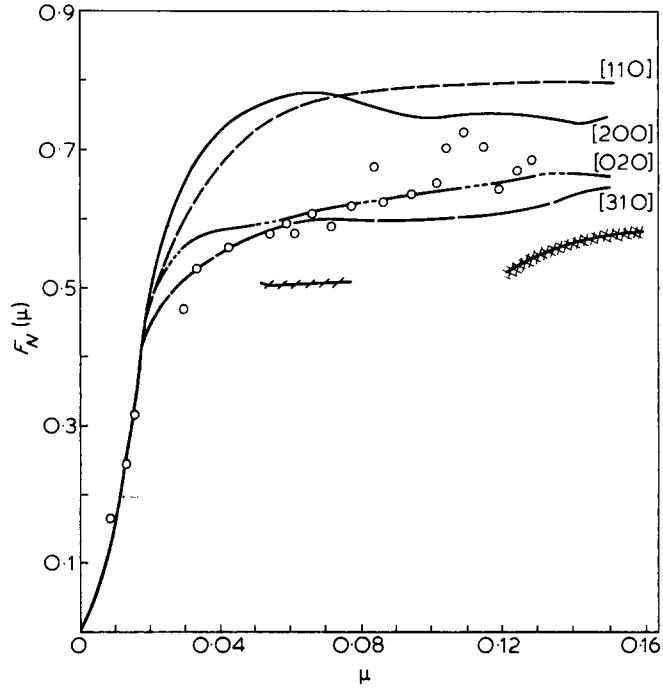

Figure 8 Scattering displayed as $F_N(\mu)$ *versus* μ for the central core model for various fold planes. (O) is explained in *Figure 3*

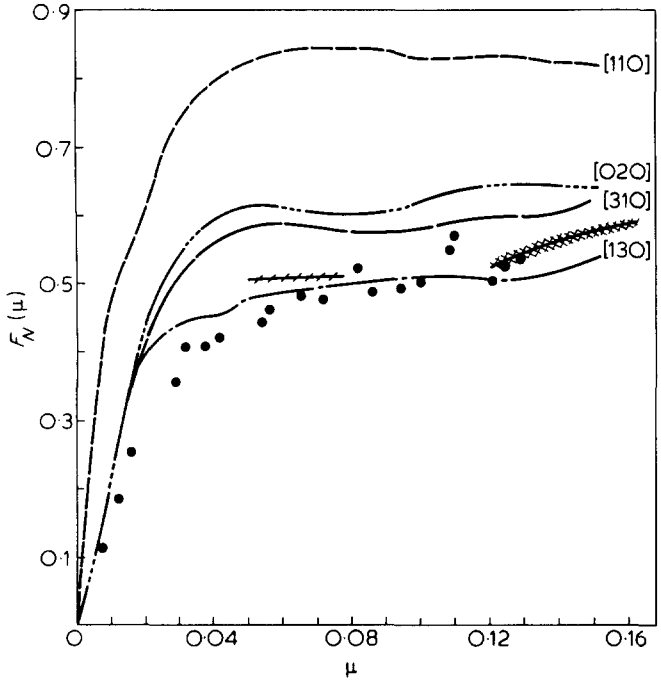

Figure 9 Scattering displayed for $F_N(\mu)$ *versus* μ for the central core model for $N = 2500$ for various fold planes

pletion process (i.e., the consecutive filling in of niches with stems) is in principle different for the other fold planes that we have employed. The concept of substrate completion with adjacent re-entry is as valid for the accretion of stems in 'niches' in say the [020] plane as it is in the [110] or [200] plane. (See also previous remarks concerning [330] plane growth in i-polystyrene single crystals.)

ROUGHENING OF FOLD PLANE

In crystallization from dilute solutions the electron microscope evidence shows that the growing edge of the crystal is rougher the larger the undercooling. This macro roughening can be viewed as arising from microscopic surface roughing which may arise from many nuclei (or niches) forming simultaneously along the growth edge. When the niches (or nuclei) are widely separated we have smooth edges but as we decrease the nuclei or niche separation we begin to roughen the fold surface. The regime theory of Hoffman and Lauritzen[9,10,27] explains nicely the features of edge roughening. The roughening one sees in solution growth crystals at large undercoolings may be expected in melt grown crystals at large undercoolings and for the quenched melt crystallized samples used in the SANS work one is at very high effective undercoolings deep into regime II, or even in Regime III[28]. Here one expects, as discussed by Hoffman *et al.*[9], an occurrence of nucleation niches at very close distances [2.0 nm (20 Å) or less]. As a result one expects for crystallization in this regime significant fold plane roughening.

It is clear that rough edges are consistent with diminished adjacent re-entry, although they do not unambiguously demand it. The superfolding model advanced by Sadler *et al.*[2,29] and suggested by Sanchez and DiMarzio in another context[29] can result in roughness with perfect adjacent re-entry. However the simultaneous incorporation of niches requires that for n niches per molecule there be at least $n-1$ non-adjacent stems. We therefore proceed to a modelling of surface roughness which allows for non-adjacent re-entry.

We have tried to take surface roughness into account in modelling the SANS. In *Figures 10* and *11* we show the nearest possible energetically favoured sites for stems to be laid down (at niches) on a surface roughened fold plane for [110], [200], [020], and [310] folding. In each figure we go to the nearest possible neighbour which has the minimum energy (or a niche) for a surface roughening resulting from a single plane roughening jump and a double plane roughening jump. No other roughening jumps were allowed for the calculations.

In order to estimate the roughening, one needs to determine what fraction of the steps remains on the fold plane itself, jumps to the nearest plane and jumps to the next nearest plane, etc. This has not been done. Instead, in the calculation we assumed 50% remained on the same plane adjacent, 25% went to the next plane and 25% made a jump of two planes. Clearly for any realistic system more or less roughening than this is possible. Nonetheless no other fractions of roughening were assumed. In *Figures 12*, *13* and *14*, the effect of roughening on the SANS intensity for the two chain morphological models is shown for roughening of the [110], [200], [310], and [020] folds.

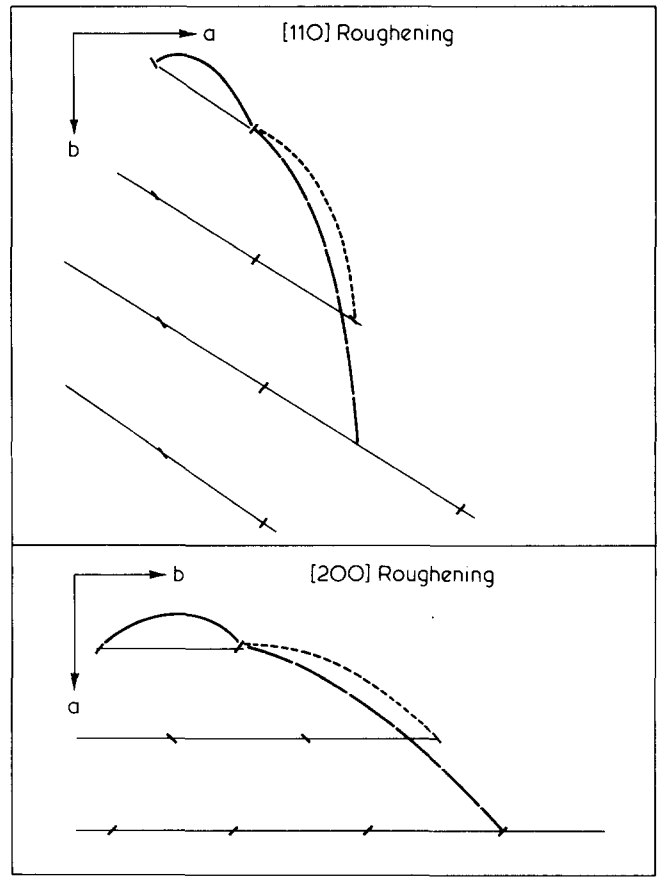

Figure 10 Schematic representation of modes of fold plane roughening. Shown above are schematics for energetically favourable and closest roughening of the [110] and [200] fold plane. Loops are folds for folding on same plane (—), then roughening one fold plane away (— — —) and finally for roughening with a two plane jump (— — —). Straight lines connect stems (/) in the same fold plane

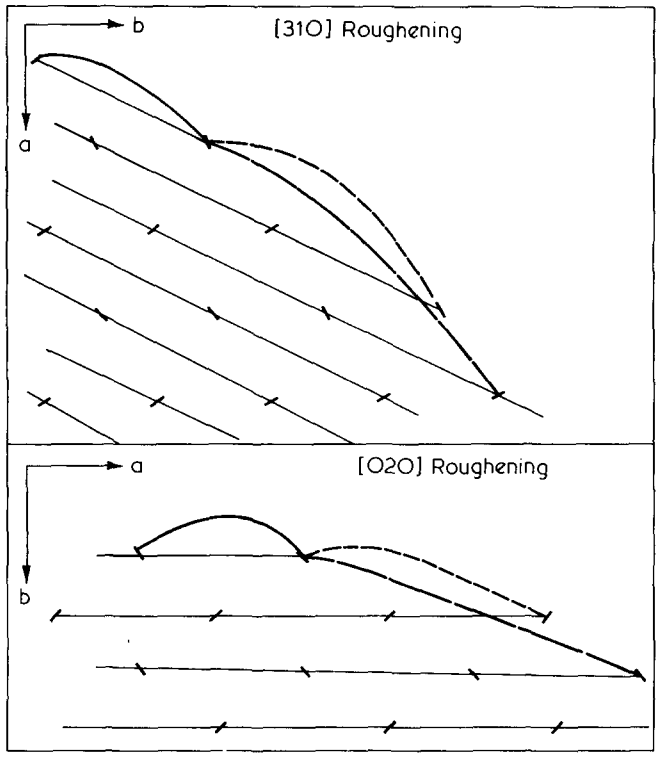

Figure 11 Schematic representation of modes of fold plane roughening. Shown above are schematics for energetically favourable and closest roughening of the [310] and [020] fold plane. Loops are folds for folding on same plane (——), then roughening one fold plane away (— — — —) and finally for roughening with a two plane jump (—— —— ——). Straight lines connect stems (//) in the same fold plane

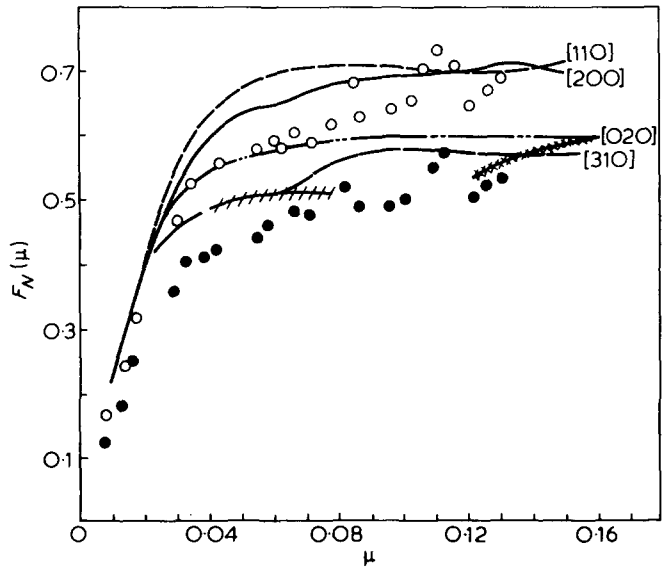

Figure 12 Scattering displayed as $F_N(\mu)$ *versus* μ for the variable cluster model where we have allowed roughening of the [110], [200], [020], and [310] fold planes. For all the data displayed, 50% of the folds remain in the same plane, 25% jump to the next fold plane and 25% jump to the fold plane two planes away.

Scattering from both these folded models for [110] and [200] folding in the variable cluster model brings this scattering relatively close to the g.p.c. scaled Schelten data as does the scattering with these roughened fold planes for the central cluster model with ten stems in the central cluster. The scattering from [020] and [310] planes roughened with these models seems to agree with the SANS scaled Schelten data.

MODELS WITH DISTRIBUTIONS OF TIGHT FOLDS

In an earlier paper it was suggested that a combination of tight folds with adjacent and near adjacent re-entry would cause no density anomaly[16,19]. In that earlier work it was shown that Sadler's[18] leapfrog model of one-third near fold, one-third next near and one-third next next near folds

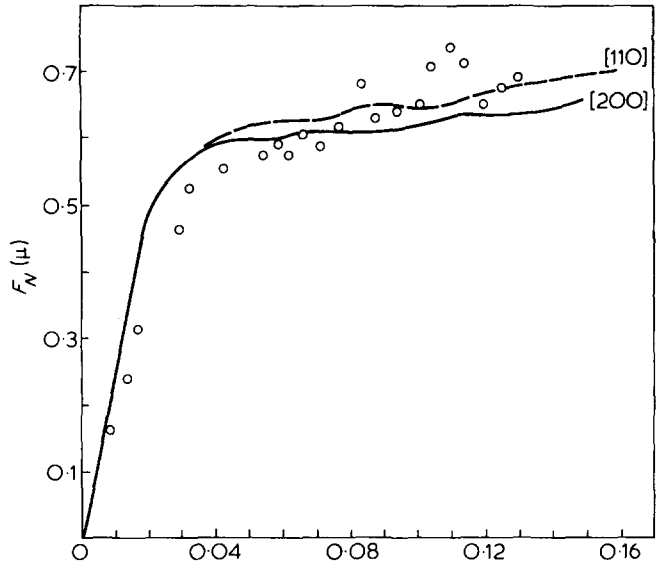

Figure 13 Scattering displayed as $F_N(\mu)$ *versus* μ for the central core model with N = 3500 where we have allowed roughening of the [110] and [200], fold planes. For all the data displayed 50% of the folds remain in the same plane, 25% jump to the next fold plane and 25% jump to the fold plane two planes away away.

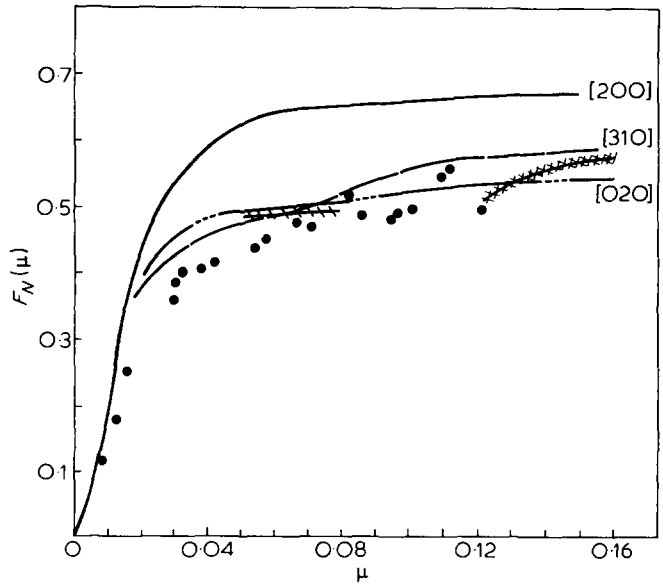

Figure 14 Scattering displayed as $F_N(\mu)$ *versus* μ for the central core model N = 2500 where we have allowed roughening of the [200], [020] and [310] fold planes. For all the data displayed 50% of the folds remain in the same plane, 25% jump to the fold plane two planes away

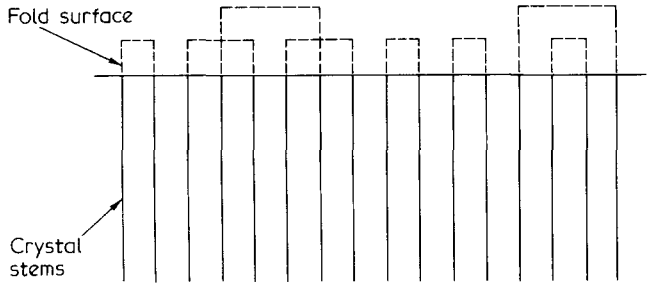

Figure 15 Schematic representation of fold surface when modelled as Sadler leapfrog model with 50% adjacent, 25% near adjacent and 25% next near adjacent

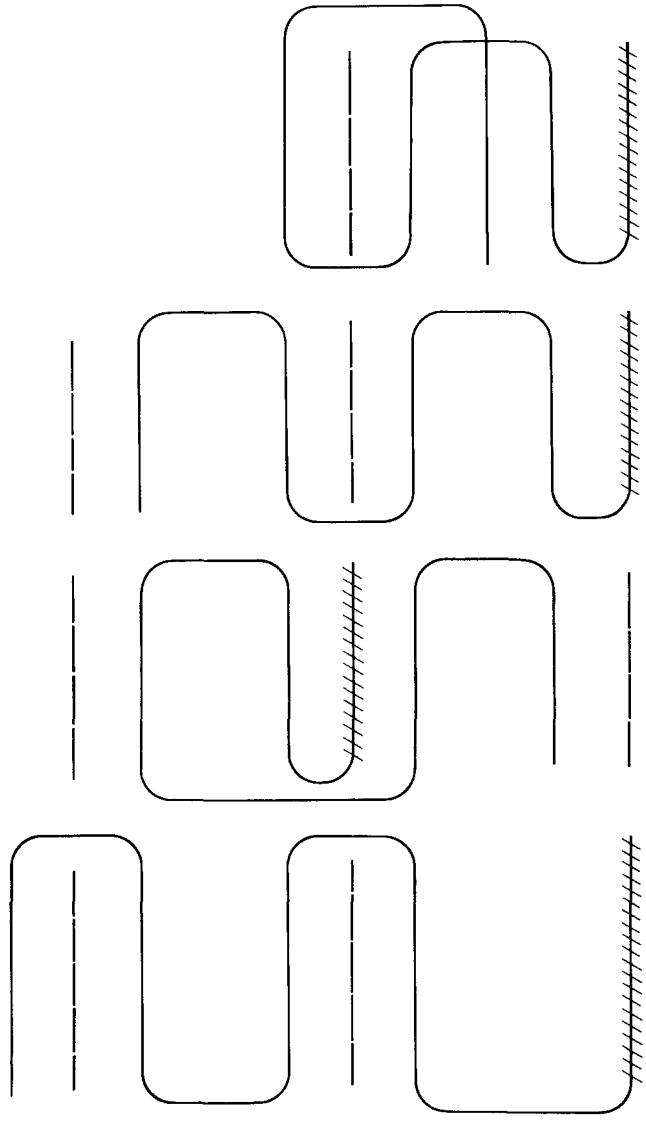

Figure 16 Various possible configurations arising from the de Gennes shadow due to reptation and the niches at 20 Å or so. Such configurations would be expected on energetic grounds at large undercooling due to the occurence of niches at close distances. Such configurations would lead to leapfrog like configurations. (*) are nucleation sites of deuterated stems. Lines (—) are deuterated chains leapfrogging along lamellae. Line (– – –) is protonated niches

showed an acceptable density profile. *Figure 15* shows a schematic of this type of tight folding where we have allowed one-half adjacent folding and only one-quarter near adjacent and one-quarter next near adjacent folds. Although Sadler[18] has proposed this model of the folding, no one has yet proposed a physical or kinetic mechanism which explains how such leapfrogging can come about. Here we propose such a mechanism.

de Gennes[31] has suggested that the deposition of a single stem by reptation leads to the occurrence of a 'shadow' stem not attached to the crystal but some 1.0–1.5 nm (10–15 Å) away from the original stem. If the reptation tube does not have time to adjust, as might occur for large undercoolings (rapid growth), then the occurrence of stems at sites 1.0–1.5 nm (10–15 Å) from the first stem should be more probable than sites at distances closer or farther. Furthermore at the large undercoolings used to prepare the SANS samples, Hoffman *et al.*[9] have argued that nucleation sites (niches) should occur at ~1.5–2.0 nm (15–20 Å). Thus at these undercoolings one would expect to have a considerable number of configurations like those depicted in *Figure 16* rather than only simple adjacent folding. Many of these models look very much like the leapfrog model for a single chain as in *Figure 15*.

We compute the SANS intensity for the leapfrog model with 50% adjacent, 25% near adjacent and 25% next near adjacent configurations. The choice of the kind of tight fold is made randomly but with the probabilities of 50%, 25% and 25%; also the direction in which we place the folds is always the same. Hence our classification of this type of fold as a 'tight' or 'regular' fold; such folds do not contribute to a surface density anomaly, but the stems associated with it are farther apart than occur with simple adjacent re-entry. The irregular folds that comprise simple non-adjacent re-entry fall in random directions from the point of emergence, and are not tight, but instead are space-filling random coils. The computation is done on both the central core model and the variable cluster model and is presented in *Figures 17*, *18* and *19*. For such models the [110] fold and the [200] fold fit the g.p.c. scaled Schelten data while the scattering from the [020] and the [310] leapfrog easily fit the SANS scaled Schelten data.

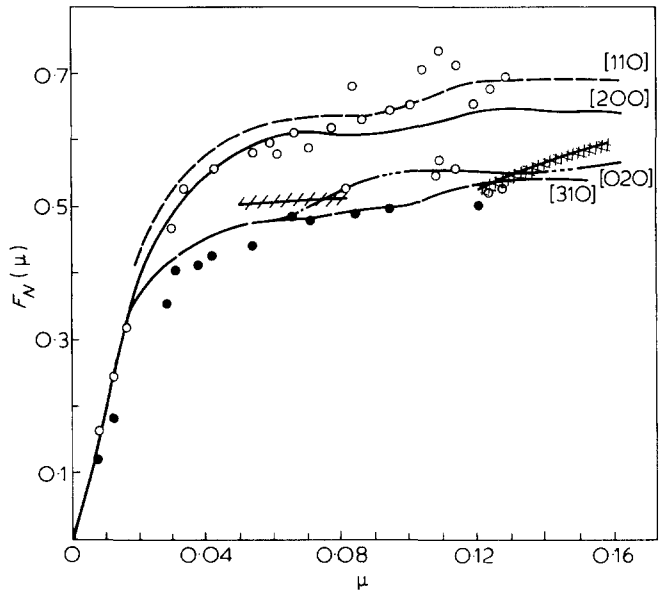

Figure 17 Scattering displayed as $F_N(\mu)$ *versus* μ for variable cluster model where the folding on the surface obeys the leapfrog model of tight folding. We show scattering intensities where leapfrogging occurs on [110], [200], [020] and [310] fold plane. For data displayed 50% of folds are adjacent, 25% are next adjacent and 25% are next next adjacent.

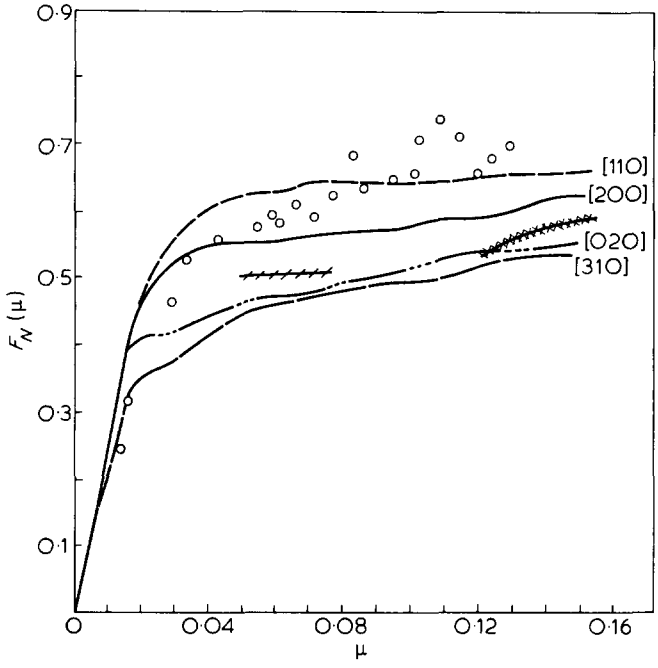

Figure 18 Scattering displayed as $F_N(\mu)$ *versus* μ for central core model with N = 3500 where the folding on the surface obeys the leapfrog model of tight folding. We show scattering intensities where leapfrogging occurs on [110], [200], [020] and [310] fold plane. For data displayed 50% of folds are adjacent, 25% are next adjacent and 25% are next next adjacent.

DISCUSSION AND CONCLUSIONS

The calculations in the previous sections show that one can match the SANS scattering intensity from $\mu = 0.01$ to $\mu = 0.14$ for models with fold planes other than the [110] and [200] fold planes or with a 'leapfrog' model which invokes tight adjacent and near-adjacent folds or with the fold plane roughening of the [110], [200], [310], or [020] fold plane. Unlike certain other calculations in the literature, scattering from the amorphous phase as well as from the stems in the crystal was considered. None of the models invoked in this paper has the serious density anomaly of the switchboard or random re-entry model. All of the models described here do have high probabilities of adjacent or near adjacent re-entry and close to the correct experimental C_n and degree of crystallinity.

Theories of Hoffman *et al.* also suggest that these models are consistent with ideas which can be derived from the kinetic theory of crystallization with chain folds in the form that includes reptation[9,28] as the transport mechanism in the melt. In brief, crystallization at large undercoolings is on the basis of the kinetic theory apt to produce niches that are quite close together [$\sim$2.0 nm (20 Å)] which promotes non-adjacent re-entry on the maximum scale in a lamellar system[9]. The lower theoretical limit[16-18] for tight folding $p_{tf} \simeq 2/3$ is therefore closely approached in specimens crystallized in the manner described, and non-adjacent re-entry at the same time approaches its theoretical maximum of one third. Meanwhile, the kinetic theory for large undercoolings, which we label Regime III[28], suggests that the adjacent stems will appear in clusters of variable size between the niches, the average cluster size consisting of roughly 2–4 adjacent stems. We also observe that the growth front in Regime III is expected to be rough because of the numerous closely spaced surface nuclei. This nucleation theory is consistent with the variable cluster model. At higher crystallization temperatures, e.g., Regime II, the niches are further apart on the growth front, and longer runs of adjacent stems are possible, though not necessarily required. Accordingly both the variable cluster model and the central core models are appropriate choices for tests for material crystallized in Regime II. The specimens used in neutron scattering experiments have in general not been characterized carefully enough with respect to the actual growth temperature range to be sure whether Regime II or Regime III growth was involved.

We wish to re-emphasize that the samples of PEH–PED that have been used for the SANS measurements are, owing to the difficulty in preparing solid solutions of PED in PEH, rapidly quenched samples. Under such conditions of quenching (or undercooling) one would not necessarily expect adjacent folding on the [110] and [200] plane as is usually found at small undercoolings in single crystals formed from solution. In fact, fold planes other than the [110] and [200] plane have been invoked to explain various observations in solution and melt grown polyethylene. Furthermore, theoretical developments[10] in polymer crystallization argue that the edge surface roughening may occur at high undercoolings. Finally, others proposed the leapfrog model to explain data on single crystals and we have offered a mechanism which might cause the leapfrogging. Thus, we have offered reasons for the invoking of our new models which do not depend on the SANS experiments alone.

One might in the final analysis find that not any one of these effects —different fold planes, fold plane roughening or the inclusion of some 'leapfrogging' structures —taken singly is the ultimate explanation of the scattering but that some combination of them is effective and represents the true chain morphology. While a number of factors, including the uncertainties in the data, preclude making a

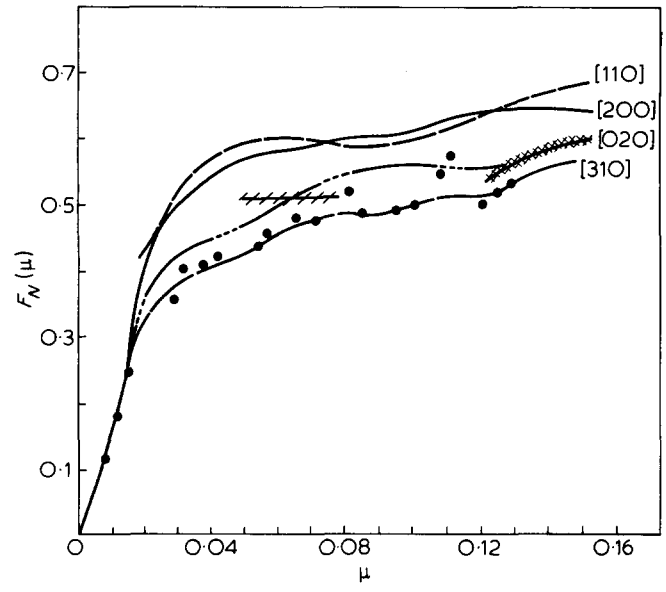

Figure 19 Scattering displayed as $F_N(\mu)$ *versus* μ for central core model with N = 2500 where the folding on the surface obeys the leapfrog model of tight folding. We show scattering intensities where leapfrogging occurs on [110], [200], [020] and [310] fold planes. For data displayed 50% of folds are adjacent, 25% are next adjacent and 25% are next next adjacent.

final choice at this juncture, it is possible to provide some evaluation concerning which of the models presented are physically the most likely.

As noted above, we regard it as quite probable, on independent grounds, that the growth front is highly roughened. Meanwhile, we see no reasonable objection to the concept that some 'leapfrogging' occurs. Given this situation, then both the central core or variable cluster models with folding on a [310] growth plane or the central core and variable cluster models with roughening and/or leapfrogging with [110] or [200] or some mixture of these fold planes, give a good account of the Schelten g.p.c. data. On the other hand if the Schelten SANS data (and the data of other investigators that resemble it) is thought to be better, then the central core or variable cluster models with substantial [310] folding with roughending and/or leapfrogging is indicated. The choice can, with only a little additional uncertainty, be narrowed further. It has been established experimentally that the radius of gyration of quench-crystallized polyethylene exhibits a liquid-like radius of gyration that varies as $M^{1/2}$ over a considerable range of molecular weight, with little deviation except at quite low molecular weights[32]. As has been shown by Guttman[8], the variable cluster model has the interesting natural property of exhibiting a C_n or radius of gyration that is practically identical to that of the interpenetrated random-coil melt from which the crystalline lamellae were formed. The radius of gyration in the crystallized state thus varies as $M^{1/2}$ for the variable cluster model. No special assumptions are required to obtain this result. The central core model does not exhibit a radius of gyration that varies as $M^{1/2}$ unless the assumption is made that the number of stems in core increases with molecular weight. While such behaviour is possible, it strikes us as reasonable to give some preference to the variable cluster model because it leads naturally to a radius of gyration that varies in the manner found experimentally in the general range of molecular weights of interest here.

Accordingly we believe it reasonable to give some emphasis to the variable cluster model with surface roughening and/or leapfrogging with the fold planes [110], [200], and [310], or some mixture thereof, being given consideration. This suggestion refers to quench-crystallized polyethylene of the type used in the SANS investigations. We would expect the central core model to become applicable for material formed at higher crystallization temperatures. Unfortunately this point cannot be checked for polyethylene, since the PED and PEH segrate at small undercoolings. It is again worth noting that i-polystyrene crystallized from the melt at relatively high temperatures appears to conform to a model of the central core type[6]. It must be understood that the chain morphology in a lamellar system is among other things a function of the undercooling at which the lamellae were formed from the melt: the disorder associated with the fold surface will be at a maximum for quench-crystallized specimens of the type used in the SANS investigations on polyethylene mentioned in this paper.

Despite the uncertainties in the exact molecular conformation for quench-crystallized polyethylene, one overall conclusion stands out: It is evident that the probability of tight or 'regular' folding p_{tf}, is close to 0.7. This interesting result is practically model-independent, as a survey of the calculations in this paper and those given elsewhere shows. It is essentially a foregone conclusion that $p_{tf} \simeq 0.7$ once it has been decided that a density anomaly cannot be tolerated at the lamellar surface. Even considering the differences between the experimental results of various investigations, the valid SANS analyses (i.e. those that do not exhibit density anomalies) always appear to point to about this amount of regular folding. We regard this as a useful general conclusion.

We see no reason to accept models of a lamellar crystal that are switchboard-like, the 'fold' surface disorder being characterized by random or nearly random re-entry with $p_{tf} \sim 0$, this phenomenon presumably being occasioned by an inability to disentangle even a few consecutive stems from the melt. The SANS results mitigate strongly against such models, since $p_{tf} \sim 0.7$, and it has further been shown[9,22] that reptation provides a highly effective mechanism for transport of enough segments from the melt to the crystal surface to form groups of adjacent stems such as appear for instance in the variable cluster model. We find it reassuring in this connection that theoretical estimates give the lower bound $p_{tf} \simeq 2/3$[16,17]. This result is rigorous for the case where the stems are perpendicular to the lamellar surface.

The probability of 'tight' or 'regular' folding consists of two contributions. The first and larger of these is the probability of strictly adjacent re-entry on a specified fold plane, p_{ar}. The SANS results for polyethylene are consistent with values of p_{ar} of ~ 0.4–~ 0.7. The other contribution to 'tight' or 'regular' folding consists of (a) tight folds that form traverses between adjacent sites on fold planes with different crystallographic indices as can occur on a rough growth front and (b) the longer but tight folds that can occasionally occur that skip one or two sites and then re-enter the same fold plane. The SANS results on polyethylene are consistent with probabilities (a) and (b) above summing up to at most ~ 0.3. The probability of true non-adjacent re-entry, $p_{nar} = 1 - p_{tf}$ is about 0.3 for polyethylene that is quench-crystallized from the melt. We emphasize again that the results quoted here represent a 'worse case' for regular chain folding in the sense that the specimen preparation used in the SANS experiments on polyethylene was conducive to a close approach to the maximum degree of surface disorder in a semicrystalline lamellar system.

The subject of the number of interlamellar links has not been discussed, but we consider it useful to mention that the present analysis does not generally alter our previous conclusions[8] on this topic. As a reference point, we indicate that all of the models presented here are consistent with the presence of roughly one interlamellar link for each molecule for $MW = 5 \times 10^4$. Thus, about one surface site in 20 involves a link to another lamella. Such a result is at strong variance with many pictorial representations[12] but in good accord with the independent estimates of Backman[33] obtained by e.s.r. studies on fracture surfaces of quench-crystallized lamellar polyethylene and with the results obtained from the Gamblers Ruin[16,17] model of the chain in the amorphous phase of a semicrystalline polymer.

ACKNOWLEDGEMENTS

We would like to acknowledge helpful discussions with Drs F. McCrackin, C. C. Han and F. Khoury.

REFERENCES

1 Schelten, J., Ballard, D. G. H., Wignall, G. D., Longman, G. and Schmaltz, W. *Polymer* 1976, **17**, 751
2 Sadler, D. M. and Keller, A. *Macromolecules* 1977, **10**, 1128 and Comments by Sadler, D. M. in *Faraday Soc. General Discussion No 68*, 1979
3 Stamm, F., Fisher, E. W., Dettenmaier, M. and Covent, P. *Faraday Soc. General Discussion No. 68*, 1979, 263
4 Bai, S. J. *Thesis* 1979, Univ. of Michigan; also see Summerfield, G. C., King, J. C. and Ullman, R. *J. Appl. Cryst.* 1978, **11**, 534
5 Ballard, D. G. H., Schelten, J., Crowley, T. L. and Longman, P. W. *Polymer* 1979, **20**, 399
6 Guenet, J. M., Picot, C. and Benoit, H. *Faraday Soc. General Discussion No. 68*, 1979, **251**, also see Guenet, J. M. *Macromolecules* 1980, **22**, and Guenet, J. M. and Picot, C. *Polymer* 1979, **20**, 1483
7 Guttman, C. M., Hoffman, J. D. and DiMarzio, E. A. *Faraday Society General Discussion No. 68*, 1979, **177** and comments by Guttman, C. M. in that volume
9 Hoffman, J. D., DiMarzio, E. A. and Guttman, C. M. *Faraday Soc. General Discussion No. 68* (in press)
10 Hoffman, J. D., Davis, G. T. and Lauritzen, J. I. in 'Treatise on Solid State Chemistry' (Ed. N. B. Hannay) Plenum Press, New York, 1970, Vol 3, ch 7
11 Yoon, D. Y. and Flory, P. J. *Faraday Soc. General Discussion No. 68* 1979, **452**
12 Yoon, D. Y. and Flory, P. J. *Polymer* 1976, **18**, 509
13 Flory, P. J. *J. Am. Chem. Soc.* 1962, **84**, 2857
14 Khoury, F. and Passaglia, E. 'Treatise on Solid State Chemistry' (Ed. N. B. Hannay) Plenum Press, New York, 1976, Vol 3, ch 6
15 Frank, C. *Faraday Soc. General Discussion No. 68* 1979, **7**
16 DiMarzio, E. A. and Guttman, C. M. *Polymer* 1980, **21**, 733
17 Guttman, C. M. and DiMarzio, E. A. *Bull. Am. Phys. Soc.* 1980, **25**, 318; Guttman, C. M., DiMarzio, E. A. and Hoffman, J. D., to be published
18 Sadler, D. *Faraday Soc. General Discussion No. 68* 1979, **106**
19 DiMarzio, E. A., Guttman, C. M. and Hoffman, J. D. *Polymer* 1980, **21**, 1379
20 Flory, P. J. 'Statistical Mechanics of Chain Molecules', Interscience Publishers, 1969
21 de Gennes, P. G. *Macromolecules* 1976, **9**, 591
22 DiMarzio, E. A., Guttman, C. M. and Hoffman, J. D. *Faraday Soc. General Discussion No. 68* 1979, **198**
23 Klein, J. and Ball, R. C. *Faraday Soc. General Discussion No. 68* (in press)
24 Keller, A. *Reports on Prog. in Physics* 1969, **XXXI**, 623
25 Bassett, D. C. and Keller, A. *Phil. Mag.* 1962, **7**, 1553
26 Krimm, S. *Proc. Int. Symp. Macromolecules, Rio de Janeiro, July 26–31, 1974* (Ed. E. B. Mano), Elsevier, Amsterdam, 1974, p 107
27 Hoffman, J. D. and Lauritzen, J. I. *J. Appl. Phys.* 1973, **44**, 4346
28 Hoffman, J. D., Guttman, C. M. and DiMarzio, E. A. *Polymer* to be published
29 Sadler, D., Comments in *Faraday Soc. General Discussion No. 68* (in press)
30 Sanches, I. C. and DiMarzio, E. A. *J. Chem. Phys.* 1971, **55**, 893
31 de Gennes, P. G. *Faraday Soc. General Discussion No. 68* 1979, **381**
32 Ballard, D. G. H., Burgess, A. N., Crowley, T. C., Longman, G. W. and Schelten, J. *Faraday Soc. General Discussion No. 68* 1979, **279**
33 Backman, D. K. and DeVries, K. L. *J. Polym. Sci., A-1* 1979, **7**, 2125